



Eddy Detection in the Marginal Ice Zone with Sentinel-1 Data Using YOLOv5

Eduard Khachatryan ^{1,*}, Nikita Sandalyuk ^{2,†} and Pigi Lozou ^{3,†}

¹ Department of Physics and Technology, UiT The Arctic University of Norway, NO-9037 Tromsø, Norway

² Department of Oceanology, Saint Petersburg State University, 199034 Saint Petersburg, Russia; n.sandalyuk@spbu.ru

³ School of Electrical and Computer Engineering, National Technical University of Athens, 15780 Athens, Greece; el16431@central.ntua.gr

* Correspondence: eduard.khachatryan@uit.no

† These authors contributed equally to this work.

Abstract: The automatic detection and analysis of ocean eddies in the marginal ice zone via remote sensing is a very challenging task but of critical importance for scientific applications and anthropogenic activities. Therefore, as one of the first steps toward the automation of the eddy detection process, we investigated the potential of applying YOLOv5, a deep convolutional neural network architecture, to specifically collected and labeled high-resolution synthetic aperture radar data for a very dynamic area over the Fram Strait. Our approach involved fine-tuning pre-trained YOLOv5 models on a sparse dataset and achieved accurate results with minimal training data. The performances of the models were evaluated using several metrics, and the best model was selected by visual examination. The experimental results obtained from the validation and test datasets consistently demonstrated the robustness and effectiveness of the chosen model to identify submesoscale and mesoscale eddies with different structures. Moreover, our work provides a foundation for automated eddy detection in the marginal ice zone using synthetic aperture radar imagery and contributes to advancing oceanography research.

Keywords: mesoscale eddies; submesoscale eddies; eddy detection; marginal ice zone; deep learning; YOLOv5; CNNs



Citation: Khachatryan, E.; Sandalyuk, N.; Lozou, P. Eddy Detection in the Marginal Ice Zone with Sentinel-1 Data Using YOLOv5. *Remote Sens.* **2023**, *15*, 2244. <https://doi.org/10.3390/rs15092244>

Academic Editors: Angelo Perilli, Mariona Claret and Alexandre Stegner

Received: 20 March 2023

Revised: 18 April 2023

Accepted: 22 April 2023

Published: 24 April 2023



Copyright: © 2023 by the authors. Licensee MDPI, Basel, Switzerland. This article is an open access article distributed under the terms and conditions of the Creative Commons Attribution (CC BY) license (<https://creativecommons.org/licenses/by/4.0/>).

1. Introduction

Eddies play a key role in ocean dynamics by encapsulating and transporting large amounts of water and their associated physical and biochemical properties over long distances. This has a significant impact on ocean circulation, heat uptake, gas exchange, carbon sequestration, and nutrient transport [1,2]. As one of the most important elements of the climate system, a single eddy may transport trillions of tons of water and tens of terajoules of heat from their generation regions to the dissipation site, thus having a significant influence on climate variability and predictability [1]. Eddies dominate the kinetic energy of the ocean over horizontal distances of tens to hundreds of kilometers and play a major role in vertical and horizontal mixing, such as cross-frontal exchange [3]. The detailed study of mesoscale eddies is crucial for better understanding dynamic, climatic, and biological ocean processes.

A marginal ice zone (MIZ) is a transition region from the open sea to dense drift ice. The MIZ is characterized by strong lateral buoyancy gradients, energetic atmosphere–ice–ocean interactions, and enhanced biological productivity [4]. The formation of eddies at the MIZ is a common dynamic feature that plays an important role in the various exchange processes of mass, heat, and momentum. These eddies can affect the position of the ice edge and biological productivity within the MIZ [5,6].

To this day, the data from altimetry missions are the main sources of information about mesoscale variability in the World Ocean. The accumulation of decades-long global altimetry time series, the development of gridded altimetry products from multiple missions, and the implementation of various automated eddy identification algorithms have enabled oceanographers to obtain an unprecedented amount of statistical information on various eddy properties and their propagation characteristics, such as the number of generated eddies, their geometric and physical properties, and translation velocities [1,7]. However, the altimetry data have significant limitations in the polar regions. Arctic eddies are several times smaller in size than low-latitude eddies, and the gridded altimetry AVISO fields resolve only a small fraction of eddies in the polar regions with typical radii of 30–50 km [8]. Consequently, spatial scales under 30 km are essentially unobserved. Moreover, the conventional way of using the altimetry data for eddy observation is complicated in the polar regions by the presence of sea ice, which makes this data type almost inapplicable for eddy detection in the MIZ.

Eddy-resolving models with a resolution of 1 km or finer are important sources of data on the mesoscale/submesoscale dynamics in the polar regions. Models such as FESOM make it possible to study the dynamics of small eddies near the sea ice edges [8,9]. However, eddy-resolving Arctic Ocean simulations are computationally demanding and require actual data as part of an observational basis for model improvement and validation [9]. For MIZ regions, this information is still very limited due to the scarcity of in situ observations, spatial and temporal limitations of altimetry data, and weather restrictions of optical satellite data.

Currently, the most universal source of information about eddy dynamics in polar regions is remote sensing data obtained from synthetic aperture radar (SAR). High-resolution SAR images can resolve ocean dynamics at scales of 0.1–1 km, and they are weather and cloud independent. SAR signatures of sea ice are well sustained under any weather conditions, making them nearly perfect for monitoring eddy dynamics in MIZ regions. Eddies manifest themselves on SAR images via three main mechanisms: wave-current interactions that modulate short-scale surface roughness patterns, near-surface wind variations across oceanic fronts, and the accumulation of slicks and ice floes in the MIZ [10,11]. Since our work considers eddies in the MIZ region, the presence of sea ice is an underlying condition for the efficiency of the developed method of eddy detection.

It should be emphasized that other sensors can potentially be used for eddy monitoring, such as optical sensors that provide images in visible and infrared channels of the electromagnetic spectrum [12]. The main advantage of optical images is easier visual interpretability, especially in comparison to SAR data. Additionally, similar to SAR, optical data are usually provided in high spatial resolution, allowing for the identification of smaller eddies and sea ice formations and structures on the underlying surface. However, the most crucial limitation of such data is their high sensitivity to atmospheric and light conditions, which is a significant problem for the Arctic region where cloud cover and long periods of darkness prevail for several months of the year [13]. Therefore, optical sensors can only be partially used depending on the data availability and final application [14].

Numerous studies have used SAR images for eddy detection in MIZ [4,8,10,15]. However, the underlying methodology for all these studies is based on visual inspection of satellite images, which is time-consuming, strongly relies on expert knowledge, and is prone to various biases and errors. Based on decades of experience in eddy identification from satellite data, it is clear that for the accumulation of a significant amount of statistical data on eddy properties in MIZ regions, it is necessary to develop a robust methodology for automated eddy identification from SAR images. It should also be noted that in recent years, several studies have implemented various machine learning algorithms for eddy detection from SAR images [16–19]. However, all of these studies were focused on identifying eddies in ice-free zones. In contrast, our study is focused on the MIZ region where the main eddy tracers are different types of sea ice, which require a completely new approach for eddy detection.

The study area is located over the Fram Strait, which is a 600 km wide passage between the Svalbard archipelago and Greenland, representing a unique deep-water connection

between the Arctic and the rest of the world. The water mass exchange is controlled by two main currents: West Spitsbergen Current (WSC) and the East Greenland Current (EGC). Fram Strait is an ideal place to study eddies in the MIZ, due to the fact that this is one of the most dynamic regions and it is the main gateway through which sea ice leaves the Arctic Ocean.

The rest of this paper is organized as follows. Section 2 demonstrates the dataset description. Section 3 shows the method used in this study. Section 4 presents an analysis and experimental results. Finally, the discussion and conclusions are presented in Section 5.

2. Dataset Description

The following section describes the dataset used in this study. The dataset was generated from Sentinel-1 imagery in an extra-wide (EW) swath mode at dual-polarization (HH and HV). Sentinel-1 operates at the C-band with a central frequency of 5.404 GHz and includes two polar-orbit Sentinel-1A and Sentinel-1B missions that are able to work at multiple sensing modes. There are several crucial things that motivated us to specifically use Sentinel-1. First and foremost is the complete independence of atmospheric and light conditions, which is particularly significant when operating in polar regions. The second major benefit is that Sentinel-1 can provide high-resolution imagery with a pixel size of 40 m, which allows us to visually identify eddies with different sizes and distinguish smaller structures on the surface. Moreover, it is worth emphasizing that Sentinel-1 data are publicly available through Copernicus Open Access Hub, the European Union's Earth observation program. Accordingly, the Sentinel-1 data were corrected for thermal noise and calibrated to sigma nought in dB using the ESA Sentinel-1 Toolbox.

The collected dataset includes 25 scenes, from June to November 2022, which cover the melting and ice formation season over the area of the Greenland Sea, East Greenland. The aforementioned scenes were partitioned into two distinct sets: a training set consisting of 20 scenes, and a validation set consisting of 5 scenes, for the purpose of training and evaluating the neural network. It should be noted that the validation dataset includes four scenes with eddies in the MIZ that will be further demonstrated. The 5th one is the open ocean image with various ocean signatures, which was employed to make sure that the detection algorithm will not fail in the scenario with no eddies in the MIZ. Moreover, we collected a few additional scenes, which were not labeled in order to test the proposed architecture. Figure 1 illustrates the study area along with the false-color composites that were used for training.

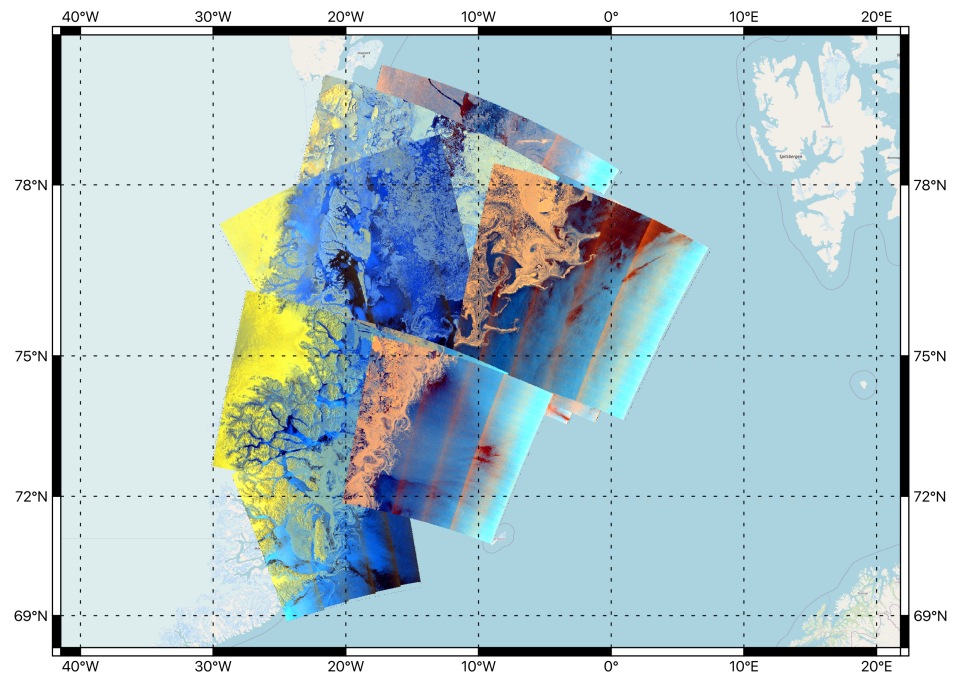


Figure 1. Study area over the Greenland Sea, East Greenland, as well as false-color composite representations of SAR images (HV, HH, and HH-HV, as RGB) illustrating the total coverage of all the images used in this study.

Figure 2 illustrates a few eddy signature examples that were used for training. It is evident that eddies in the MIZ, especially on SAR images, can look very different depending on many parameters. In this paper, we are focusing on detecting all of the eddy signatures. However, in future studies, we will plan to distinguish and detect different types of eddies in terms of their size, shape, and rotation direction.

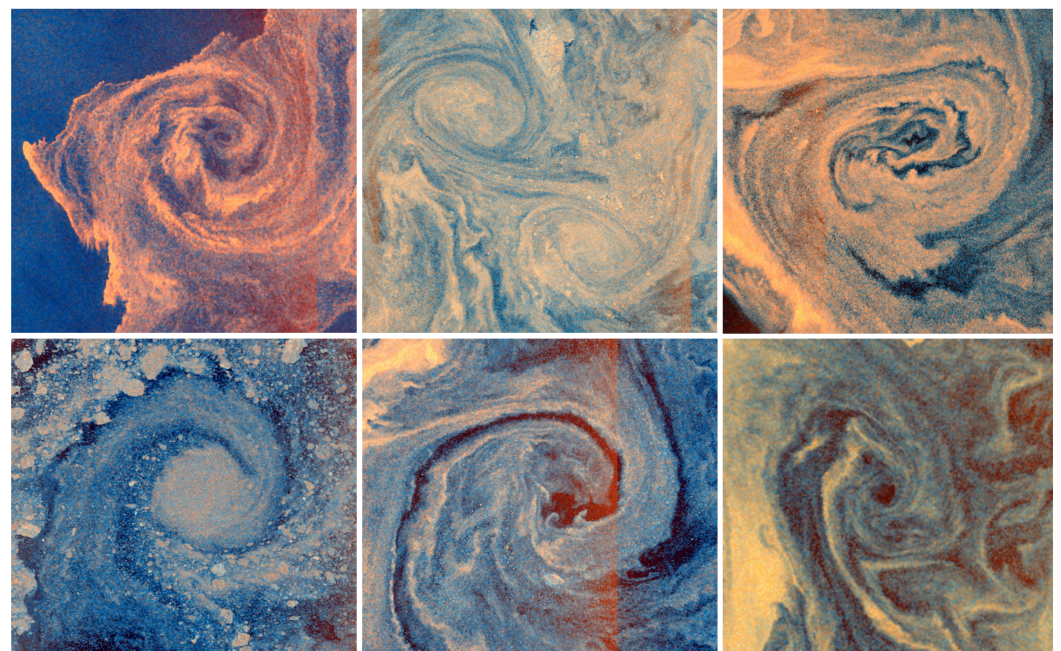


Figure 2. Example of different eddies in the MIZ that were used for the training part of this study.

3. Method Description

In this study, we trained different YOLOv5 [20] models for the purpose of eddy detection in the MIZ. YOLOv5 is a state-of-the-art object detection algorithm that can detect

and locate objects in an image or video in real time with high accuracy. It is the latest version of the YOLO (You Only Look Once) family of object detection models, and it was introduced in 2020 by Ultralytics. YOLOv5 uses a deep convolutional neural network architecture that is trained on the common objects in context (COCO) dataset [21], an extensive dataset of labeled images to identify various objects, such as people, animals, vehicles, etc.

The YOLOv5 network uses a combination of convolutional, upsampling, and specialized layers to identify objects with varying scales and aspect ratios [20]. The network is composed of a backbone feature extractor, a neck, and a head. The backbone is a pre-trained network that extracts rich feature representations from images, reducing spatial resolution and increasing channel resolution. YOLOv5 uses CSP-Darknet53 as its backbone, which combines CSPNet [22] and Darknet-53 [23]. Darknet-53 is a 53-layer convolutional neural network used for feature extraction, while CSPNet solves the issue of redundant gradients in large-scale backbones, such as Darknet, by truncating gradient flow. This reduces the number of parameters and computation required, improving inference speed, which is crucial for real-time object detection [22]. The neck module includes a spatial pyramid pooling (SPP) [24] module that maximizes input pooling and group features of different scales. This allows the model to generalize well to objects of different sizes and scales. The model head is a convolutional neural network that performs final operations, applying anchor boxes on feature maps to render the final output: classes, scores, and bounding boxes.

There are several various sizes of YOLOv5 that cater to different use cases and requirements. YOLOv5 nano (YOLOv5n) and YOLOv5 small (YOLOv5s) are the smallest and fastest variants of YOLOv5, with smaller model sizes and fewer layers. They are suitable for applications that require real-time object detection on low-powered devices. YOLOv5 medium (YOLOv5m) has a medium-sized model with more layers and higher accuracy than YOLOv5s. It is suitable for applications that require higher accuracy while still maintaining real-time performance. YOLOv5 large (YOLOv5l) has a larger model size and more layers than YOLOv5m, which results in even higher accuracy but at the cost of slower inference speed. It is suitable for applications that require the highest possible accuracy. YOLOv5 x-large (YOLOv5x) has the largest model size and the most layers of all YOLOv5 variants. It achieves the highest accuracy among all YOLOv5 models but at the cost of a slower inference speed and higher memory requirements. It is suitable for applications that require the highest possible accuracy and have access to high-performance computing resources.

In order to select the best-performing YOLOv5 model, the five different models were trained using the specified training set and evaluated using the validation set for up to 500 epochs each. It is worth noting that our dataset for eddy detection is substantially small, which presents a challenge for training accurate object detection models. In order to address this challenge, we chose to fine-tune pre-trained YOLOv5 models for eddy detection.

During training, the model learns to predict bounding boxes around eddies and calculates a confidence score for each predicted box. To evaluate the accuracy of the models, the mean average precision (mAP) metric was used, with a confidence threshold range of 50% to 95%. The mAP is a commonly used metric in object detection [25] that measures the accuracy of the model in detecting objects at different levels of confidence. Specifically, it calculates the average precision (AP) for each class of object detected and then takes the mean across all classes to arrive at an overall mAP score.

In the present case, the model with the highest mAP score was selected for each architecture.

4. Experimental Results & Discussion

The following section demonstrates the comparison of different YOLOv5 models along with a performance of fine-tuned YOLOv5s on the validation and test datasets for the detection of eddies in the MIZ.

4.1. Comparison

To optimize training efficiency, the false-color composites were resized to 1500×1500 pixels. This allowed the models to be trained faster without sacrificing accuracy. To compute the models, NVIDIA T4 Tensor Core GPUs were used, which were available through Google Colab.

In Table 1, we present the metrics of the best models for each architecture. The detection results of these models on the validation set were compared, revealing that YOLOv5x had superior overall metrics. Figure 3 displays the output of the YOLOv5 small, large, and x-large deep-learning algorithms, featuring the detected eddy signatures in the MIZ. The green boxes indicate the correctly detected eddies, while the red boxes represent missed eddies. Cyan boxes denote eddies that were not initially labeled but were subsequently detected by the algorithm. This validation image serves as a suitable example of why we prefer YOLOv5s for eddy detection. Although larger architectures have higher metrics due to their superior performance in detecting more difficult eddies, YOLOv5s is an efficient and lightweight model that excels in detecting the most obvious eddies. Moreover, YOLOv5s outperformed YOLOv5x in detecting more prominent eddies. Therefore, we selected YOLOv5s for our specific application of eddy detection.

Table 1. Comparison of different YOLOv5 models on the validation dataset.

YOLOv5	Precision	Recall	mAP50	mAP50-95
nano	0.769	0.500	0.512	0.235
small	0.867	0.500	0.622	0.255
medium	0.685	0.556	0.594	0.284
large	0.862	0.556	0.638	0.289
x-large	0.872	0.611	0.653	0.290

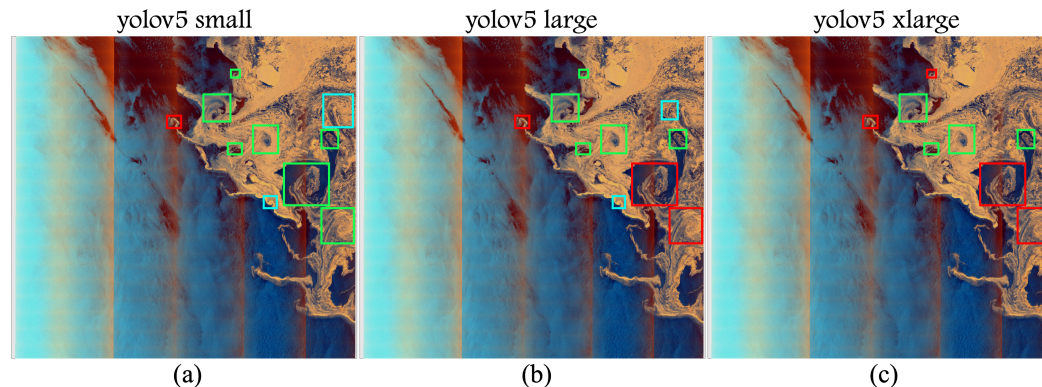


Figure 3. Comparison of the best YOLOv5 models according to Table 1, namely YOLOv5 small (a), large (b), and x-large (c) for the scene acquired on 8 September 2022. Green boxes display the correctly detected eddies, red boxes show eddies that were missed by the architecture, and the cyan boxes illustrate eddies that were not initially labeled but were detected by the algorithm.

4.2. Validation Dataset

Figure 4 illustrates the output of the YOLOv5s deep-learning model, which was used to detect eddy signatures in the MIZ from SAR false-color composites. The algorithm was evaluated using a validation dataset, which consisted of labeled eddies. Green boxes show the correctly detected eddies, while the missed eddies are demonstrated with red boxes. Additionally, the cyan boxes illustrate the eddies that were not initially labeled but were detected. It is evident from the images that we were able to highly minimize the false alarm detections by choosing the right deep-learning architecture. Even though the eddy signatures on the SAR false-color composites vary significantly in terms of shape and size, especially in the MIZ, almost all of the labeled eddies were properly detected. While the individual small submesoscale eddies were missed by the chosen model in Figure 4a,d, in Figure 4b, the algorithm missed a lower part of the dipole eddy. Moreover, some of the

eddy signatures were not initially labeled, however, they were detected by the algorithm, which is especially clear in Figure 4c.

Sea ice acts as Lagrangian particles, and in the vast majority of cases, the algorithm was able to perfectly capture the eddy shape spiraling signatures and identify the core and most of the peripheral areas of the vortex structure. Based on the data from the validation dataset, the algorithm detects eddies in the spatial scale range from 1 to 100 km, thus covering both the mesoscale and submesoscale ranges.

The ocean eddies manifest themselves on the ocean surface via different geometrical forms. They can be very close to the circular shape, which poses no problem for the algorithm. However, in certain cases, the eddies take elongated shapes and even stretch into filaments due to interactions with background currents that are inhomogeneous in space [26]. In some cases, the algorithm detects such filament structures, which cannot be fully avoided since most of the filaments have a high value of vorticity and are even visually almost inseparable from the main eddy field. Additionally, the elongated shapes of the eddies lead to the impossibility of detection of the peripheral part of the eddies.

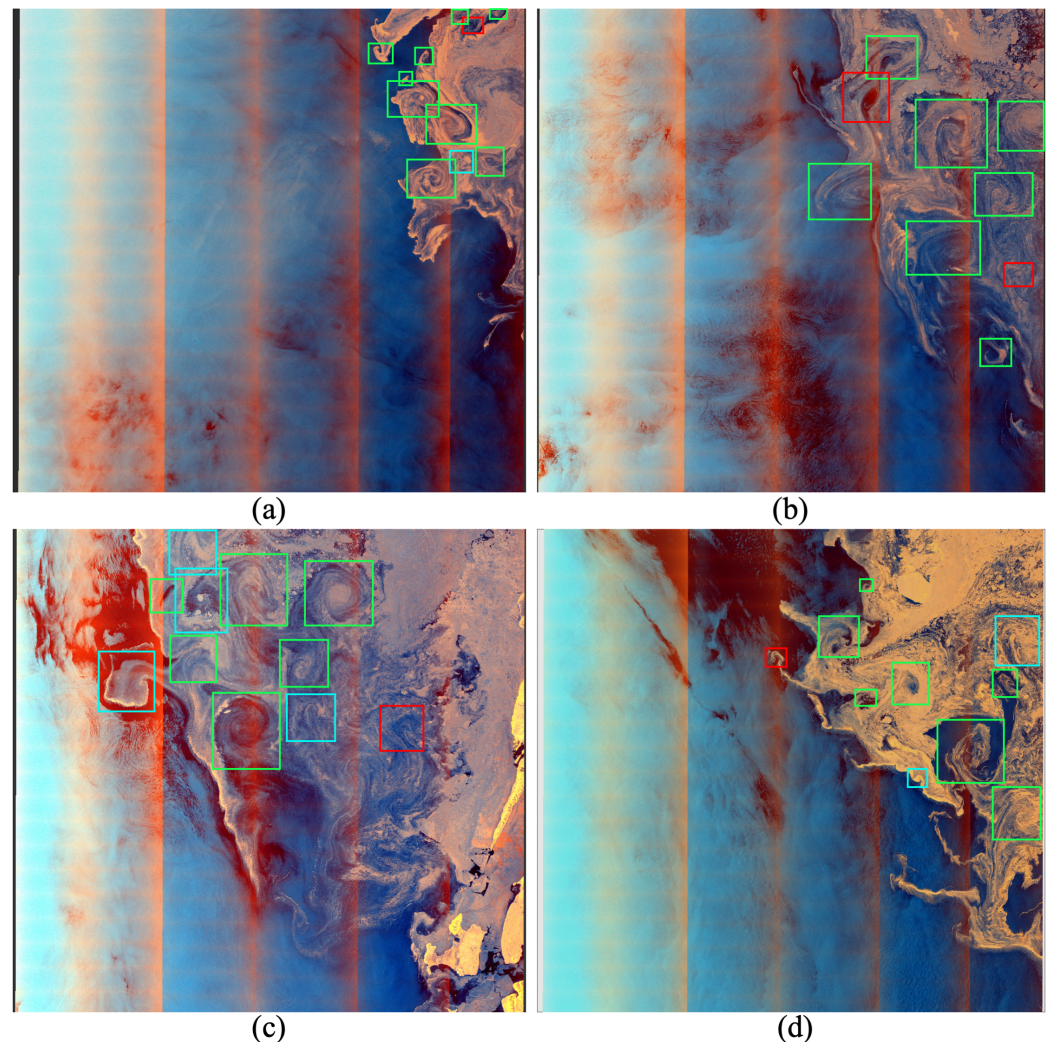


Figure 4. The outputs of the algorithm with detected eddies in the MIZ for (a) 28 June, (b) 27 July, (c) 30 July, and (d) 8 September 2022. Green boxes illustrate the correctly detected eddies, red boxes demonstrate eddies that were labeled but were missed by the architecture, and the cyan boxes show the eddies that were detected by the algorithm but were not initially labeled.

The eddy boundary in the high turbulent areas, such as MIZ, is diffusive and cannot be correctly identified with the approach used in our work. There are different methods for

eddy boundary detection [1,7] and it usually demands the implementation of the physical or geometrical criteria, which is out of the scope of this study.

While identifying eddies is a complex task due to their intricate geometric configurations, recent advancements in machine learning offer exciting opportunities to overcome these challenges. Although labeling eddies demands specialized expertise, resulting in a limited dataset and uncertainties in labels, we are confident that we can obtain high-quality labeled data with modern techniques. Furthermore, integrating other sensors with a coarser spatial resolution can expand the dataset and improve the accuracy of our model. Although there may be some misdetections in our current approach, they can be resolved through further investigation and improvement in future studies. We believe that our approach will provide valuable insights and contribute to the advancement of eddy detection using machine learning.

4.3. Test Dataset

Here, we present the outputs of the YOLOv5s algorithm for detecting eddies in the MIZ over the East Greenland Coast. The test data used for this analysis were acquired on (a) 27 November and (b) 9 December 2022. The detected eddies are highlighted in green boxes in Figure 5, demonstrating the ability of the algorithm to robustly detect eddy signatures with different structures.

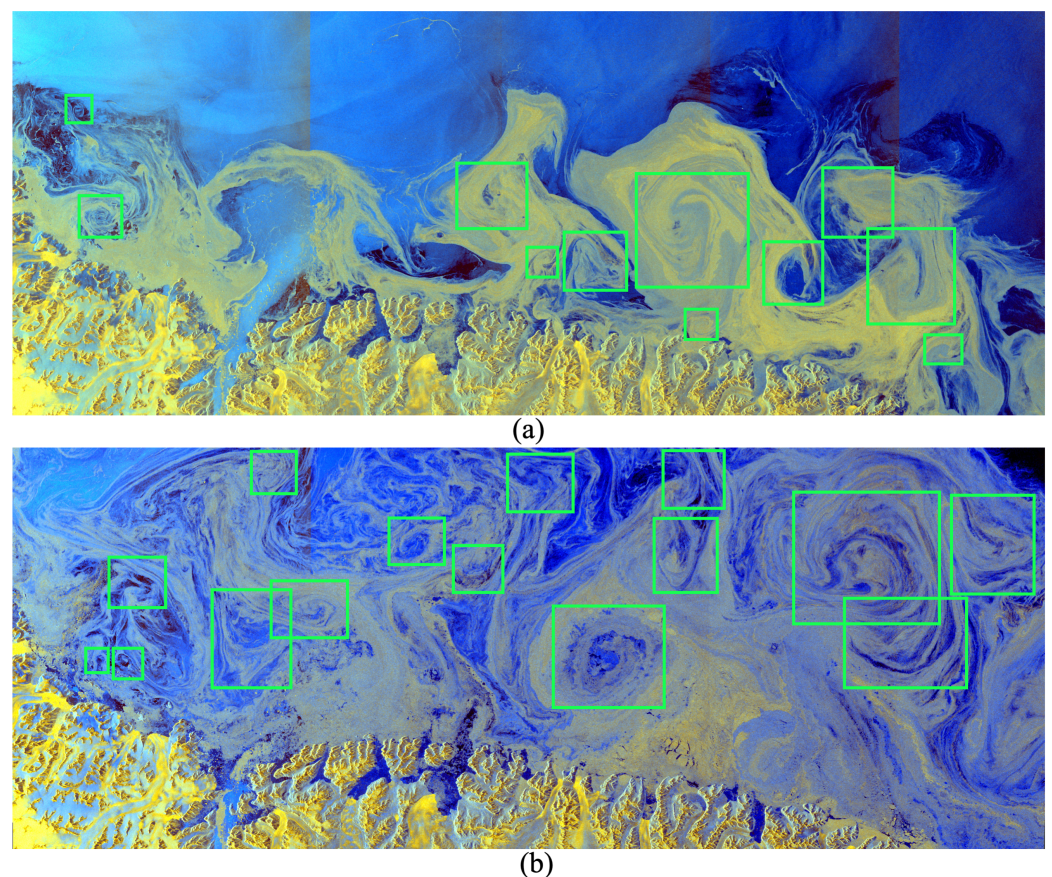


Figure 5. The example of the YOLOv5 outputs with the detected eddies in the MIZ for test data acquired on (a) 11 November and (b) 9 December 2022 over the East Greenland Coast. Green boxes demonstrate eddies that were detected by the algorithm.

One of the major advantages of using YOLOv5 for eddy detection is its ability to perform real-time processing of the image data. This allows for the timely detection of eddies, which is critical in various applications, such as polar navigation, offshore operations, and oceanographic observations. The results of our experiments using YOLOv5s consistently

demonstrate the robust detection of eddies in the MIZ, which is a crucial first step toward automating the eddy detection process.

5. Conclusions

In this paper, we demonstrate the first step towards the automatization of eddy detection in the MIZ. Specifically, we focused on the MIZ areas where the main tracers of eddies are different types of sea ice, mainly brash ice. This is a narrow field that has not been extensively studied, requiring a new approach to eddy detection. The experimental results obtained from both the validation and test datasets consistently demonstrated the effectiveness and robustness of the chosen deep learning architecture in identifying submesoscale and mesoscale eddies with various shapes. This reveals the huge potential of deep-learning algorithms for such a challenging task as eddy detection in the MIZ.

SAR data were utilized in this work for eddy detection in the MIZ for several crucial reasons, such as independence of light and weather conditions, high spatial resolution, and public availability. The eddies on the SAR imagery can be detected due to the difference in surface roughness between the sea ice and open water boundary. Nevertheless, other instruments can be used, namely sea surface temperature sensors, satellites equipped with altimeters, and optical sensors. Each of these sensors has its own advantages and limitations. As a future step, we will consider integrating various sources of data since combining data from different instruments can potentially improve the understanding of the interactions between the ocean and the sea ice as well as the formation of eddies for a particular region.

While the primary goal of this study is to select and optimize the appropriate architecture for detecting all eddy signatures without further discrimination based on size (submesoscale or mesoscale), shape, or rotation direction (anticyclonic or cyclonic), future research will mainly focus on distinguishing and detecting various eddy types in the MIZ.

Overall, the results presented in this study illustrate the effectiveness and robustness of YOLOv5 in detecting eddies in the MIZ, providing a promising foundation for future research in automating the detection of eddies in various marine environments.

Author Contributions: Visualization, formal analysis, and writing: all authors. Methodology: P.L. Supervision: N.S. and E.K. Data collection: E.K. Data labeling: N.S. and E.K. All of the authors participated in the discussion and the review of the manuscript. All of the authors contributed equally to this work. All authors have read and agreed to the published version of the manuscript.

Funding: This work is funded by the Centre for Integrated Remote Sensing and Forecasting for Arctic Operations (CIRFA) and the Research Council of Norway (RCN grant no. 237906).

Data Availability Statement: Sentinel-1 SAR data used in this study, are publicly available on the Copernicus Open Access Hub at <https://scihub.copernicus.eu>, accessed on 17 December 2022.

Acknowledgments: The article contains Sentinel-1 Copernicus data.

Conflicts of Interest: The authors declare no conflict of interest.

Abbreviations

The following abbreviations are used in this manuscript:

SAR	synthetic aperture radar
EW	extra-wide
MIZ	marginal ice zone
EGC	East Greenland Current
WSC	West Spitsbergen Current
YOLOv5	you only look once version 5
COCO	common objects in context
AP	average precision
mAP	mean average precision

References

1. Chelton, D.B.; Schlax, M.G.; Samelson, R.M. Global observations of nonlinear mesoscale eddies. *Prog. Oceanogr.* **2011**, *91*, 167–216. [CrossRef]
2. Wunsch, C. Where do ocean eddy heat fluxes matter? *J. Geophys. Res. Ocean.* **1999**, *104*, 13235–13249. [CrossRef]
3. Thomas, L.N.; Tandon, A.; Mahadevan, A. Submesoscale Processes and Dynamics. In *Ocean Modeling in an Eddying Regime*; American Geophysical Union (AGU): Washington, DC, USA, 2008; pp. 17–38. [CrossRef]
4. Kozlov, I.E.; Plotnikov, E.V.; Manucharyan, G.E. Brief Communication: Mesoscale and submesoscale dynamics in the marginal ice zone from sequential synthetic aperture radar observations. *Cryosphere* **2020**, *14*, 2941–2947. [CrossRef]
5. Johannessen, J.A.; Johannessen, O.M.; Svendsen, E.; Shuchman, R.; Manley, T.; Campbell, W.J.; Josberger, E.G.; Sandven, S.; Gascard, J.C.; Olaussen, T.; et al. Mesoscale eddies in the Fram Strait marginal ice zone during the 1983 and 1984 Marginal Ice Zone Experiments. *J. Geophys. Res. Ocean.* **1987**, *92*, 6754–6772. [CrossRef]
6. Von Appen, W.J.; Wekerle, C.; Hehemann, L.; Schourup-Kristensen, V.; Konrad, C.; Iversen, M.H. Observations of a Submesoscale Cyclonic Filament in the Marginal Ice Zone. *Geophys. Res. Lett.* **2018**, *45*, 6141–6149. [CrossRef]
7. Faghmous, J.; Frenger, I.; Yao, Y.; Warmka, R.; Lindell, A.; Kumar, V. A daily global mesoscale ocean eddy dataset from satellite altimetry. *Sci. Data* **2015**, *2*, 150028. [CrossRef] [PubMed]
8. Bashmachnikov, I.; Kozlov, I.; Petrenko, L.; Glock, N.; Wekerle, C. Eddies in the North Greenland Sea and Fram Strait From Satellite Altimetry, SAR and High-Resolution Model Data. *J. Geophys. Res. Ocean.* **2020**, *125*, e2019JC015832. [CrossRef]
9. Wang, Q.; Koldunov, N.V.; Danilov, S.; Sidorenko, D.; Wekerle, C.; Scholz, P.; Bashmachnikov, I.L.; Jung, T. Eddy Kinetic Energy in the Arctic Ocean From a Global Simulation With a 1-km Arctic. *Geophys. Res. Lett.* **2020**, *47*, e2020GL088550. [CrossRef]
10. Kozlov, I.E.; Artamonova, A.V.; Manucharyan, G.E.; Kubryakov, A.A. Eddies in the Western Arctic Ocean From Spaceborne SAR Observations Over Open Ocean and Marginal Ice Zones. *J. Geophys. Res. Ocean.* **2019**, *124*, 6601–6616. [CrossRef]
11. Johannessen, J.A.; Kudryavtsev, V.; Akimov, D.; Eldevik, T.; Winther, N.; Chapron, B. On radar imaging of current features: 2. Mesoscale eddy and current front detection. *J. Geophys. Res. Ocean.* **2005**, *110*. [CrossRef]
12. Elachi, C.; van Zyl, J. *Introduction to the Physics and Techniques of Remote Sensing*; Wiley Series in Remote Sensing and Image Processing; Wiley: Hoboken, NJ, USA, 2006.
13. Sandven, S.; Johannessen, O.M.; Kloster, K. Sea Ice Monitoring by Remote Sensing. *Encycl. Anal. Chem.* **2006**, *1993*, 1–43. [CrossRef]
14. Khachatryan, E.; Sandalyuk, N. On the Exploitation of Multimodal Remote Sensing Data Combination for Mesoscale/Submesoscale Eddy Detection in the Marginal Ice Zone. *IEEE Geosci. Remote Sens. Lett.* **2022**, *19*, 1–5. [CrossRef]
15. Kozlov, I.E.; Atadzhanova, O.A. Eddies in the Marginal Ice Zone of Fram Strait and Svalbard from Spaceborne SAR Observations in Winter. *Remote Sens.* **2022**, *14*, 134. [CrossRef]
16. Karimova, S. An approach to automated spiral eddy detection in SAR images. In Proceedings of the 2017 IEEE International Geoscience and Remote Sensing Symposium (IGARSS), Fort Worth, TX, USA, 23–28 July 2017; pp. 743–746. [CrossRef]
17. Du, Y.; Liu, J.; Song, W.; He, Q.; Huang, D. Ocean Eddy Recognition in SAR Images with Adaptive Weighted Feature Fusion. *IEEE Access* **2019**, *7*, 152023–152033. [CrossRef]
18. Zhang, D.; Gade, M.; Zhang, J. SAR Eddy Detection Using Mask-RCNN and Edge Enhancement. In Proceedings of the IGARSS 2020—2020 IEEE International Geoscience and Remote Sensing Symposium, Waikoloa, HI, USA, 26 September–2 October 2020; pp. 1604–1607. [CrossRef]
19. Xia, L.; Chen, G.; Chen, X.; Ge, L.; Huang, B. Submesoscale oceanic eddy detection in SAR images using context and edge association network. *Front. Mar. Sci.* **2022**, *9*, 2584. [CrossRef]
20. Jocher, G. Ultralytics/Yolov5: V7.0—YOLOv5 SOTA Realtime Instance Segmentation. 2022. Available online: <https://zenodo.org/record/7347926> (accessed on 11 March 2023).
21. Lin, T.Y.; Maire, M.; Belongie, S.; Hays, J.; Perona, P.; Ramanan, D.; Dollar, P.; Zitnick, C.L. Microsoft coco: Common objects in context. In Proceedings of the Computer Vision—ECCV 2014: 13th European Conference, Zurich, Switzerland, 6–12 September 2014; Proceedings, Part V 13; Springer International Publishing: Cham, Switzerland, 2014; pp. 740–755.
22. Wang, C.Y.; Liao, H.Y.M.; Wu, Y.H.; Chen, P.Y.; Hsieh, J.W.; Yeh, I.H. CSPNet: A new backbone that can enhance learning capability of CNN. In Proceedings of the IEEE/CVF Conference on Computer Vision and Pattern Recognition Workshops, Seattle, WA, USA, 14–19 June 2020; pp. 390–391.
23. Redmon, J.; Farhadi, A. Yolov3: An incremental improvement. *arXiv* **2018**, arXiv:1804.02767.
24. He, K.; Zhang, X.; Ren, S.; Sun, J. Spatial pyramid pooling in deep convolutional networks for visual recognition. *IEEE Trans. Pattern Anal. Mach. Intell.* **2015**, *37*, 1904–1916. [CrossRef] [PubMed]
25. Padilla, R.; Netto, S.L.; Da Silva, E.A. A survey on performance metrics for object-detection algorithms. In Proceedings of the 2020 International Conference on Systems, Signals and Image Processing (IWSSIP), Niteroi, Brazil, 1–3 July 2020; pp. 237–242.
26. Zhmur, V.V.; Travkin, V.S.; Belonenko, T.V.; Arutyunyan, D.A. Transformation of Kinetic and Potential Energy during Elongation of a Mesoscale Vortex. *Morskoy Gidrofiz. Zhurnal* **2022**, *38*, 466–480. [CrossRef]

Disclaimer/Publisher’s Note: The statements, opinions and data contained in all publications are solely those of the individual author(s) and contributor(s) and not of MDPI and/or the editor(s). MDPI and/or the editor(s) disclaim responsibility for any injury to people or property resulting from any ideas, methods, instructions or products referred to in the content.